Targeting P16INK4A in uterine serous carcinoma through inhibition of histone demethylation

ZHEN XIAO[1,2*], YINGYING HE[1*], CHONGYA LIU[2*], LIN XIANG[2], JINGYAN YI[2], MIN WANG[2], TINGTING SHEN[2], LANLIN SHEN[2], YIJUE XUE[2], HONG SHI[1] and PIXU LIU[2,3]

[1]Department of Obstetrics and Gynecology, First Affiliated Hospital of Dalian Medical University, Dalian Medical University, Dalian, Liaoning 116011; [2]Institute of Cancer Stem Cell, and [3]School of Pharmacy, Dalian Medical University, Dalian, Liaoning 116044, P.R. China

Received April 6, 2018; Accepted February 14, 2019

DOI: 10.3892/or.2019.7067

Abstract. Uterine serous carcinoma (USC) is a subtype of endometrial cancer. Compared with endometrial endometroid carcinoma, the majority of USC cases are more aggressive. Cyclin-dependent kinase inhibitor 2A (P16INK4A) is a canonical tumor suppressor that blocks cell cycle progression; however, P16INK4A is overexpressed in USC. The aim of the present study was to determine the role of P16INK4A in P16INK4A-positive endometrial cancer, with the hope of elucidating a novel therapeutic approach for this type of malignancy. A total of 2 endometrial cancer cell lines, ETN-1 and EFE-184, were selected for further investigation, due to them being known to express high levels of P16INK4A. Using short hairpin RNA targeting P16INK4A, P16INK4A was downregulated in these cancer cell lines. Cell viability and migration were examined via 2D/3D clonogenic and wound healing assays. Subsequently, GSK-J4, a histone demethylase inhibitor, was employed to deplete P16INK4A in these cancer cell lines and an *ex vivo* culture system of a patient-derived xenograft (PDX) endometrial tumor sample. Following P16INK4A knockdown, the proliferation and migration of ETN-1 and EFE-184 cells markedly declined. When exposed to GSK-J4, the levels of KDM6B and P16INK4A were almost completely abrogated, and the cell viability was significantly reduced in these cell lines and the *ex vivo*-cultured PDX tumor explants. The association between the levels of P16INK4A, lysine demethylase 6B (KDM6B) and the methylation status of histone 3 lysine 27 (H3K27) in these cell lines and the human USC tumor sample was also demonstrated. P16INK4A appears to be oncogenic in a number of endometrial cancer cell lines. The level of P16INK4A is associated with the methylation status of H3K27. Increased methylation of H3K27 coexists with downregulation of KDM6B and, subsequently, P16INK4A, which reduces cell proliferation and invasiveness in endometrial cancer. The observations of the present study may enable the development of a novel therapeutic strategy for P16INK4A-positive endometrial cancer, particularly USC.

Introduction

Endometrial cancer is one of the most common gynecologic malignancies globally (1). Based on the current pathological classification, endometrial cancer is primarily categorized into two types: Type I, uterine endometroid carcinoma (UEC); and type II, uterine serous carcinoma (USC). UECs, the majority of which are moderately or well-differentiated, generally have a favorable prognosis (2). However, according to some reports in 2011 and 2012, USCs, which account for 5-10% of all endometrial cancer types globally, are highly aggressive and are associated with a poor outcome (2,3).

Compared with its counterpart UEC, USC is hormone-receptor negative; thus, patients with USC rarely benefit from hormonal treatment (2). Additionally, the currently limited targeted therapies are principally designed and indicated for UEC (3). Therefore, there is an urgent requirement to identify potential targets and develop effective treatment regimens for USCs (3).

Cyclin-dependent kinase inhibitor 2A (P16INK4A), encoded by the *P16INK4A* gene (also known as *CDKN2A*), has been reported to be a tumor suppressor, as it can inhibit cyclin-dependent kinase 4/6 (CDK4/6) and cause cell cycle arrest (4,5). Thus, deficiency of P16INK4A serves an important role in the development of several types of cancer, including breast and colorectal cancer (4,6). However, a number of other studies indicate that P16INK4A is frequently overexpressed in USC tissues and may serve as a protein marker for the differential diagnosis of USC and UEC (7-9).

Correspondence to: Professor Hong Shi, Department of Obstetrics and Gynecology, First Affiliated Hospital of Dalian Medical University, Dalian Medical University, 222 Zhongshan Road, Dalian, Liaoning 116011, P.R. China
E-mail: shong60@163.com

Professor Pixu Liu, Institute of Cancer Stem Cell, Dalian Medical University, 9 Wes Part, Lvshun South Road, Dalian, Liaoning 116044, P.R. China
E-mail: pixu_liu@dmu.edu.cn

*Contributed equally

Key words: endometrial cancer, cyclin-dependent kinase inhibitor 2A, histone demethylation

Previous studies demonstrated that P16INK4A is required for cell proliferation and migration in cervical and hepatic cancer (10-12). Additionally, P16INK4A overexpression has been detected in certain types of cancer, including cervical cancer (13). Although its biological function in these tissue samples has yet to be fully elucidated, researchers have reported that P16INK4A may serve a crucial role in the survival of cervical cancer cells (11,12). Furthermore, in another study, it has been reported that P16INK4A was determined to promote the migration of liver cancer cells (10). These aforementioned observations indicate that P16INK4A may exert distinct biological effects, as a tumor suppressor or an oncogenic protein, in a tissue-specific manner.

It has been reported that P16INK4A expression is regulated by the methylation level of histone 3 lysine 27 (H3K27) (14). Targeting histone lysine demethylase (KDM) 6B by GSK-J4, a KDM6B inhibitor, increases the level of H3K27 trimethylation, which is an effective approach to curtailing P16INK4A expression and reducing cell proliferation (11). Thus, P16INK4A may be worthy of further consideration as a therapeutic target for P16INK4A-positive cancer cases.

The aim of the present study was to examine the biological functions of P16INK4A in USC and to determine whether targeting KDM6B is a viable therapeutic option for the treatment of endometrial cancer.

Materials and methods

HEK293T and endometrial cancer cell lines, cell culture and reagents. The human endometrial adenocarcinoma cell lines AN3CA, EFE-184, ETN-1, Hec1A, Hec108 and Nou-1 were obtained from the Dana-Farber/Harvard Cancer Center (Boston, MA, USA). AN3CA, EFE-184, ETN-1, Hec108 and Nou-1 cells were maintained at 37˚C in a humidified normoxic atmosphere in the presence of 5% CO_2 in RPMI-1640 (Gibco; Thermo Fisher Scientific, Inc., Waltham, MA, USA), and Hec1A cells were maintained in McCoy's 5A (Gibco; Thermo Fisher Scientific, Inc.). HEK293T cells were maintained in Dulbecco's modified Eagle's medium (DMEM; Gibco; Thermo Fisher Scientific, Inc.). All the media were supplemented with 10% fetal bovine serum (FBS; HyClone; GE Healthcare, Logan, UT, USA). Among the 6 cell lines, EFE-184 and ETN-1 cells were screened and used the two for the subsequent experiments. Palbociclib was purchased from Selleck Chemicals (Houston, TX, USA; cat. no. S1579), and GSK-J4 was obtained from MedChemExpress (Shanghai, China; cat. no. HY-15648B).

Proliferation assays. Cells were plated into 96-well plates at a density of $5x10^3$ cells/well, and incubated at 37˚C with or without increasing concentrations of palbociclib (0, 0.25, 0.5, 1, 2.5, 5 and 10 μM). Cells were harvested at 72 h after palbociclib or vehicle [dimethyl sulfoxide (DMSO)] treatment, and evaluated with a Cell Counting Kit-8 assay (Dojindo Molecular Technologies, Inc., Kumamoto, Japan), according to the manufacturer's guidelines, as previously described (15). GraphPad Prism software 5.0 (GraphPad Software, Inc., San Diego, CA, USA) was used to calculate the half-maximal inhibitory concentration (IC_{50}) values.

Short hairpin RNA (shRNA) construction. The construction of shRNA P16INK4A was performed as previously described (16). Briefly, a doxycycline-inducible shRNA system was constructed and the plasmids (~150 ng/μl) were transfected into cells with a lentivirus. The following primers were designed and synthesized by Sangon Biotech Co., Ltd. (Shanghai, China), and used for P16INK4A knockdown: shP16INK4A-1, forward, 5'-CCGGCGCACATTCATGTG GGCATTTCTCGAGAAATGCCCACATGAATGTGCGTT TTTG-3', and reverse, 5'-AATTCAAAAACGCACATTCAT GTGGGCATTTCTCGAGAAATGCCCACATGAATGTGC G-3'; and shP16INK4A-2, forward, 5'-CCGGATCAGTCA CCGAAGGTCCTACCTCGAGGTAGGACCTTCGGTGAC TGATTTTTG-3', and reverse 5'-AATTCAAAAAATCAG TCACCGAAGGTCCTACCTCGAGGTAGGACCTTCGGT GACTGAT-3'. To generate pLKO-tet-on-shRNAs targeting human P16INK4A, oligonucleotides were designed and synthesized (Sangon Biotech Co., Ltd.). Following annealination, double-stranded oligonucleotides were directly ligated with pLKO-Tet-on vector that was digested with AgeI (New England Biolabs, Inc., Ipswich, MA, USA) and EcoRI (Takara Biotechnology Co., Ltd., Dalian, China). Retroviruses were generated by transfecting HEK293T cells with pWzl plasmids and packaging DNA, A total of 1.6 μg pWzl DNA, 1.2 μg pCG-VSVG, 1.2 μg pCG-gap/pol and 12 μl Lipofectamine® 3000 (Thermo Fisher Scientific, Inc.) were used. DNA and lipid were diluted in 300 μl DMEM and mixed, and following 15 min of incubation at room temperature, they were added to one 6-cm dish that was seeded with $3x10^6$ HEK293T cells 1 day earlier at room temperature. Viral supernatant was collected 48 and 72 h after transfection. After the supernatant was filtered through 0.45-μm membrane, it was added to target cells in the presence of 8 μg/ml polybrene (EMD Millipore, Billerica, MA, USA). Lentiviruses were generated with a similar approach with the exception of HEK293T cells that were transfected with 2 μg pLKO DNA, 1.5 μg pCMV-dR8.91 (Biovector, Beijing, China) and 0.5 μg pMD2-VSVG (Biovector). Cells were selected with antibiotics at 72 h after initial infection. Puromycin (Thermo Fisher Scientific, Inc.) and blasticidine (Thermo Fisher Scientific, Inc.) were used at the final concentrations of 1.5 and 4 μg/ml, respectively. The knockdown of P16INK4A was confirmed by reverse transcription-quantitative polymerase chain reaction (RT-qPCR) analysis and western blotting for at least 3 times each. The subsequent experiments were performed immediately following the transfection.

Clonogenic assay. Following transfection with shRNA plasmids, cells were seeded into 12/24-well plates at a density of $3x10^3$/$6x10^3$ cells/well, respectively, with or without doxycycline (1 μg/μl), and cultured at 37˚C for 10 days. ETN-1 and EFE-184 cells were also plated in 6-well plates at a density of $1x10^4$ cells/well with GSK-J4 (30 μM) or DMSO, and were also cultured at 37˚C for 10 days. The culture medium RPMI-1640, containing doxycycline (1 μg/μl), GSK-J4 (30 μM) or DMSO, was changed every 3 days. After 10 days of treatment, the cells were fixed and stained with methanol and crystal violet (Sigma-Aldrich; Merck KGaA, Darmstadt, Germany) mixture (0.05% concentration at room temperature for 30 min), and

then extracted with 10% glacial acetic acid. The optical density (OD) was measured at 570 nm by EnSpire® Multimode Plate Readers (PerkinElmer, Inc., Waltham, MA, USA).

Protein isolation and western blotting. The cells not treated were collected at 80% confluence, while if treated with GSK-J4, the cells were collected at the 24 h after the treatment, and if treated with Palbociclib, they were collected at 12 h after treatment. The cells were seeded at $1x10^4$ cells/plate and maintained in 60-cm plates and were lysed on ice in radioimmunoprecipitation assay buffer supplemented with protease and phosphatase inhibitors (KGP2100; Nanjing KeyGen Biotech Co., Ltd., Nanjing, China), as previously described (17). Immunoblots were conducted using a Bio-Rad system (Bio-Rad Laboratories, Inc., Hercules, CA, USA). A total of 25 μg protein was loaded for each sample, the total protein was separated by 12% SDS-PAGE and transferred to polyvinylidene difluoride membrane (EMD Millipore). The membranes were blocked with 5% milk at room temperature for 1 h and the target proteins were probed by the following antibodies for 12 h at 4˚C: P16INK4A (OriGene Technologies, Inc., Rockville, MD, USA; cat. no. ZS-0033; 1:500), KDM6B (ProteinTech Groups, Inc., Chicago, IL, USA; cat. no. 55354-1-AP; 1:1,000), H3K27-M3 (Immunoway Biotechnology Company, Plano, TX, USA; cat. no. YM3338; 1:1,000) and H3K27-M1 (Immunoway Biotechnology Company; cat. no. YM3336; 1:1,000). Vinculin (Cell Signaling Technology, Inc., Danvers, MA, USA; cat. no. #4650; 1:1,000) was used as loading control. The membrane was lastly stained with horseradish peroxidase (HRP)-conjugated rabbit anti-sheep IgG H&L (1:5,000; ab6747; Abcam, Shanghai, China) for 2 h at 4˚C. The protein bands were then detected using a radioactive detection system (SuperLumia Enhanced Chemiluminescence kit; cat. no. K22020; Abbkine Scientific Co., Ltd., Redlands, CA, USA, www.abbkine.com). The absolute density of P16INK4A bands was later determined by ImageJ software 4.0 (National Institutes of Health, Bethesda, MD, USA). The relative density of P16INK4A was normalized to the corresponding vinculin bands. In vehicle-treated cells, the relative density of P16INK4A was assigned as 1.

RT-qPCR analysis. Total RNA was isolated from the cells with an Illustra RNAspin kit (GE Healthcare) and reverse-transcribed using a iScript cDNA synthesis kit (Bio-Rad Laboratories, Inc.), according to the manufacturer's protocols. An universal SYBR®-Green MasterMix and RT-qPCR was used to measure gene expression. Briefly, the samples were incubated for 60 min at 42˚C, 15 min at 72˚C, and stored at -20˚C. For qPCR, 1 μl of diluted RT products were mixed with 10 μl of SYBR®-Green MasterMix (Bio-Rad Laboratories, Inc.), 0.5 μl of forward and reverse primers, and 4 μl of nuclease-free water for a final volume of 20 μl, according to the manufacturer's protocols. The reactions were run on the ABI-7500 Real-Time PCR System (Applied Biosystems; Thermo Fisher Scientific, Inc.) using the conditions of 40 cycles at 95˚C for 20 sec and 60˚C for 45 sec. Actb was used as the loading control. The primers for *P16INK4A* were as follows: Forward, 5'-ATATGC CTTCCCCCACTACC-3', and reverse, 5'-CCCCTGAGCTTC CCTAGTTC-3'. The primers for Actb were: forward, 5'-CCT AGAAGCATTTGCGGTGG-3', and reverse, 5'-GAGCTA CGAGCTGCCTGACG-3'. Cq values were generated using the default analysis settings. ΔCq was defined as Cq gene of interest - Cq β-actin. ΔΔCqT was defined as ΔCq treated sample - Cq control sample. Relative quantification was calculated as $2^{-\Delta\Delta Cq}$, as described previously (18).

3D Sphere-forming cultures. As previously described (19), the cells (2,000/well) were seeded on 96-well plates coated with Matrigel (BD Biosciences; Beckon, Dickinson and Company, Franklin Lakes, NJ, USA). The cells were grown in RPMI-1640 medium supplemented with 2% FBS and 2% Matrigel, and allowed to grow for 96 h at 37˚C. The original medium was replaced with the fresh RPMI-1640 medium containing 2% FBS and 2% Matrigel additional with GSK-J4 (30 μM) or vehicle (DMSO) at this time point. For shRNA P16INK4A ETN-1 and EFE-184 cells, doxycycline was added when seeding. Over 100 colonies were scored for each condition. Quantitation of tumor spheres for structural integrity was performed after a 96-h culture.

Wound healing assay. A wound healing assay was used to evaluate the migration ability of ETN-1 and EFE-184 cells, as previously described (20). Cells were plated in 24-well plates at the density of 20,000/well and grown at 37˚C in RPMI-1640 medium supplemented with 10% FBS until confluence. A scratch was created using sterile 200 μl pipette tips. PBS was used twice to remove cell debris and fresh RPMI-1640 medium supplemented with 2% FBS was added, with or without doxycycline. The mean width of each scratch was measured using Image-Pro Plus software 4.0 (Media Cybernetics, Inc., Rockville, MD, USA).

Hematoxylin and eosin (H&E) and immunohistochemistry (IHC). For H&E, tissues were first fixed in 4% paraformaldehyde solution at room temperature for 24 h. After gradient tissue dehydration (75% for 24 h; 85% for 3 h; 95% for 1 h; 100% for 1 h; and 100% for 1 h; ethanol solution at room temperature), followed by 100% xylene to remove alcohol, the tissues were embedded in paraffin. Subsequently, paraffin-embedded tissue sections (4-μm) were dewaxed with 100% xylene at room temperature for 30 min and gradient ethanol solution (100% for 10 min; 100% for 10 min; 95% for 10 min; 80% and 10 min). Subsequently, sections were immersed in 0.5% hematoxylin (cat. no. H8070; Beijing Solarbio Science & Technology Co., Ltd., Beijing, China) for 10 min followed by 5 quick dips in 0.3% acid alcohol at room temperature. The sections were then washed with running water for 60 min. Following this, 1% of eosin (cat. no. G1100; Beijing Solarbio Science & Technology Co., Ltd.) was used for 1 min at room temperature to stain the cytoplasm. IHC was performed using P16INK4A (OriGene Technologies, Inc.; cat. no. ZS-0033; 1:200), H3K27-M3 (Immunoway Biotechnology Company; cat. no. YM3338; 1:500) and H3K27-M1 (Immunoway Biotechnology Company; cat. no. YM3336; 1:500), as previously described (21). Briefly, the IHC stainning of paraffin-embedded samples was performed using a standard Biotin-Streptavidin HRP Detection method, as previously described (https://www.cellsignal.com/contents/resources-protocols/immunohistochemistry-protocol-(paraffin)/ihc-paraffin). The 4-μm sections were deparaffinized as aforementioned and antigens in the

tissue were retrieved for 5 min. Following blocking endogenous peroxidase activity with 30% hydrogen peroxide formaldehyde solution at room temperature for 30 min, the sections were incubated with 20% normal goat serum to block non-specific binding sites for 30 min at room temperature. The primary antibody used was a polyclonal antibody against human P16INK4A protein. The samples were incubated overnight at 4˚C in a moist chamber. Following 3 washes with PBS, the sections were incubated for 30 min at room temperature with goat anti-mouse secondary IgG (dilution 1:400; cat. no. SP-9001; OriGene Technologies, Inc.). The 3,5-diaminobenzidine detection kit (OriGene Technologies, Inc.) was used for staining. Negative controls with PBS (0.01 mol/l, pH 7.4) replacing the primary antibody were also included. Finally, the tissue sections were counterstained with 0.5% hematoxylin for 1 min at room temperature, dehydrated and mounted in resinous mountant at room temperature. Digital images were captured using a light microscope (Leica Microsystems GmbH, Wetzlar, German) at a x400 magnification. The intensity of P16INK4A, H3K27M1 and H3K27M3 staining was quantified as the percentage of positive cells per high-power field. The formalin fixed paraffin-embedded tissues including malignant and normal endometrium were all obtained from First Affiliated Hospital of Dalian Medical University (Dalian, China). It was approved by the ethics committee of the hospital and written informed consent were also obtained from the patients.

Patient information, tissue preparation, patient-derived xenograft (PDX) model establishment and ex vivo culture of PDX tumor tissue. Fresh tumor tissue and 121 FFPE tumor samples from other patients (age range, 38-77 years; mean age, 56 years) with endometrial cancer were collected from the Biobank of First Affiliated Hospital of Dalian Medical University. All were processed according to the protocol approved by the Institutional Review Board of the First Affiliated Hospital of Dalian Medical University. Written informed consent was obtained from the patients. A primary tumor tissue was obtained from a 57-year-old female during hysterectomy who had been diagnosed with endometrial serous carcinoma in dilatation and curettage, a pre-operative endometrium biopsy. The fresh tumor tissue was maintained in normal saline and transported to the laboratory in 4˚C on ice. Prior to transplanting the tumor into the mice, the tumor tissue was cut into 5x5x5 mm tissue blocks. A total of 2 non obese-severe combined immunodeficiency (NOD-SCID) female mice maintained in a pathogen-free environment were used to establish the first generation of PDX mouse models. The mice, each weighing 25-30 g were provided by the Laboratory Animal Center of Dalian Medical University. The 6-week old NOD-SCID mice were raised in large plastic cages with a maximum of 6 mice/cage at 40-60% humidity and 19-23˚C. The mice were maintained on a 12/12 h light/dark period with 12-15 air exchanges/h and were fed with food and water *ad libitum*. The mice bearing xenografts were housed under standard conditions and monitored closely. During the whole experiments, a total of 8 mice were used to establish models of different generations. The PDX mouse model was constructed as previously described (22). In brief, after the mice were anesthetized with intraperitoneal injection of Tribromoethanol (avertin 1.25%), 300 mg/kg, a 1-cm scalp incision was produced on the skin near each leg. Subsequently, tissue blocks were placed into the subcutaneous space and the incisions were closed. Tumor volume, body weight, living activity and food intake were monitored every 3 days. The timing of sacrifice depended on the following two conditions: If multiple tumors were present, the monitoring was terminated when the largest tumor volume reached 1 cm^3 (with the combination of the two largest tumor size <2 cm); but if only a single tumor was observed, monitoring was terminated when the largest diameter of the tumor was near 2 cm. Therefore, sufficient tissue for the experiments could be ensured. After the mice were sacrificed with cervical dislocation and the tumor tissue was transplanted into other NOD-SCID mice, as a next generation model, the 2 mice for this experiment were the third generation. In total, 5 tumors from 8 transplanting sites (4 for each mouse) were obtained and the maximum tumor size was 1.8 cm (the single tumor appeared in that mouse). The mice were then sacrificed by decapitation and tumor specimens were used for *ex vivo* culture, as previously described (23). Briefly, the fresh tumor specimen was dissected into ~1-mm^3 tissue blocks. The blocks were cultured on an absorbable gelatin sponge in the presence of vehicle control (DMSO) or GSK-J4 (50 μM) for 24 h. All animal procedures were conducted under the approval of the Institutional Animal Care and Use Committee of Dalian Medical University (Dalian, China) and strictly followed the guideline for tumor induction in mice and rats (http://igeam.dmu.edu.cn/jgsz1/SPFdwsyzx1/zcfg.htm).

Statistical analysis. Data are expressed as mean ± standard deviation or percentage. In analyzing quantitative results, Student's t-test and χ^2 test were used for two group comparison, analysis of variance and a post hoc test (Student-Newman-Keuls) were used for multiple comparisons. $P<0.05$ was considered to indicate a statistically significant difference. All statistical analyses were performed by GraphPad Prism 5.0 software.

Results

P16INK4A is overexpressed in the majority of USC cases. To evaluate the levels of P16INK4A expression in endometrial cancer, IHC staining was performed on 121 tumor samples from patients (age range, 38-77 years, with the mean age of 56 years) with endometrial cancer at First Affiliated Hospital of Dalian Medical University. In line with the observations of previous studies (8,9,24-26), it was observed that P16INK4A was overexpressed in the majority of USC cases and was negative in the majority of UEC cases, with 75% (25/33) of USCs and 12% (11/88) of UECs being P16INK4A-positive (Fig. 1A and B, Table I). In normal endometrium from 8 individuals receiving hysterectomy due to of uterine leiomyoma, the expression of P16INK4A was negative. The representative image was depicted (Fig. 1A). Therefore, these results demonstrated that P16INK4A is overexpressed in the majority of USC samples.

Overexpression of P16INK4A acts as an oncogenic event for a number of endometrial cancer cell lines. As P16INK4A overexpression in tumor tissue contradicts its known role as a tumor suppressor, the aim was to investigate its function in endometrial cancer cells. Firstly, the expression of P16INK4A was tested in 6 endometrial cancer cell lines (AN3CA, EFE-184, ETN-1, Hec108, Hec-1A and Nou-1) and the

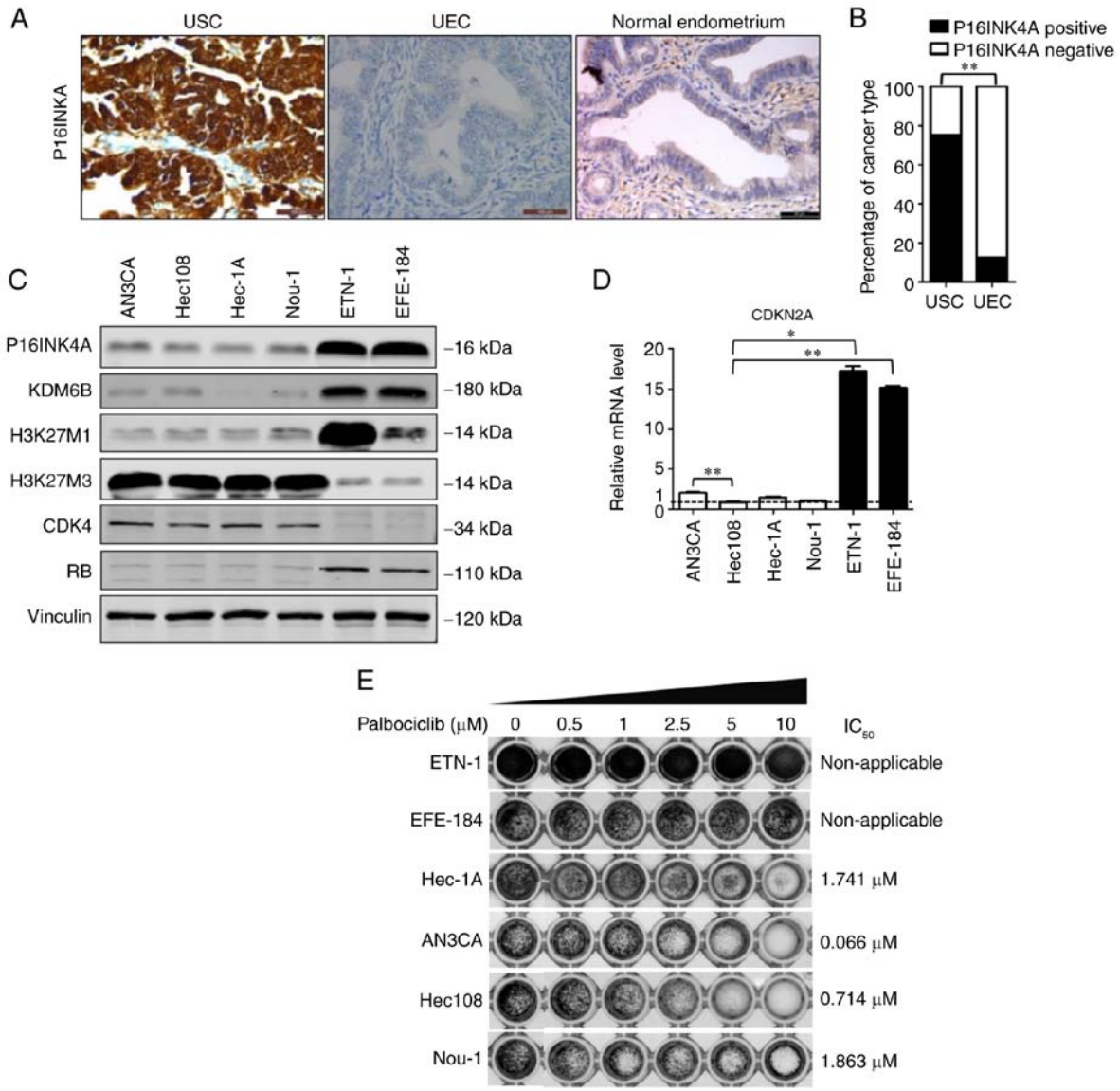

Figure 1. Differential expression of P16INK4A in tumor samples. (A) Representative images of P16INK4A positivity in USC, P16INK4A negativity in UEC and P16INK4A negativity in normal endometrium. The normal tissue was obtained from 8 patients with leiomyoma who receiving hysterectomy procedures. Scale bar, 50 μm. (B) Percentage of P16INK4A-positive cases among 33 USC and 88 UEC samples. **P<0.01 (χ^2 test). (C) Western blot analysis of 6 endometrial cell lines (AN3CA, Hec1A, Hec108, Nou-1, EFE-184 and ETN-1). Vinculin was used as a loading control. (D) The reverse transcription-quantitative polymerase chain reaction results of the 6 endometrial cell lines (AN3CA, Hec1A, Hec108, Nou-1, EFE-184 and ETN-1) were analyzed and shown as relative *P16INK4A* mRNA level of the Hec1A values, which were then converted as fold change. *P<0.05 and **P<0.01 [analysis of variance and a post hoc test (Student-Newman-Keuls)]. (E) Response of different endometrial cell lines to the CDK4/6 inhibitor palbociclib. The viability of ETN-1, EFE-184, Hec-1A, AN3CA, Hec108 and Nou-1 cells was measured with a Cell Counting Kit-8 assay following treatment with vehicle (dimethyl sulfoxide) and palbociclib (0.5, 1, 2.5, 5 and 10 μM) for 72 h. The IC_{50} are depicted. P16INK4A, cyclin-dependent kinase inhibitor 2A; CDK4, cyclin-dependent kinase 4; UEC, uterine endometroid carcinoma; USC, uterine serous carcinoma; H3K27, histone 3 lysine 27; KDM6B, histone lysine demethylase 6B; IC_{50}, half-maximal inhibitory concentration; RB, retinoblastoma.

expression level of P16INK4A was determined to be highest in ETN-1 and EFE-184 cells, whereas it was relatively low in AN3CA, Hec108, Hec-1A and Nou-1 cells (Fig. 1C and D).

Tumor suppressor retinoblastoma (RB) acts downstream of CDK4/6 and serves an important role in the cell cycle (4,5). RB-deficient tumors frequently express high levels of P16INK4A (4-6). A research group reported that, when P16INK4A is overexpressed, CDK4/6 expression is suppressed to prevent cancer cells from responding to CDK4/6 inhibitors (27). Thus, to investigate the function of CDK4/6 in the aforementioned endometrial cancer cell lines, their treatment response to the CDK4/6 inhibitor palbociclib were evaluated. Highly P16INK4A-expressing ETN-1 and EFE-184 cells were determined to be resistant to palbociclib. The remaining cell lines (AN3CA, Hec108, Hec-1A and Nou-1), in which P16INK4A expression was low or negative, were sensitive to the treatment, with an IC_{50} of 0.066, 0.714, 1.741 and 1.863 μM, respectively (Fig. 1E). Therefore, ETN-1 and EFE-184 cells were selected for further experiments.

To determine whether P16INK4A acts as a driving factor in the proliferation of ETN-1 and EFE-184 cells, P16INK4A was transfected into ETN-1 and EFE-184 cells by transfecting two P16INK4A-specific shRNAs. The downregulation of P16INK4A was verified by RT-qPCR and western blot analyses (Fig. 2A and B). Following doxycycline-induced P16INK4A depletion, the growth

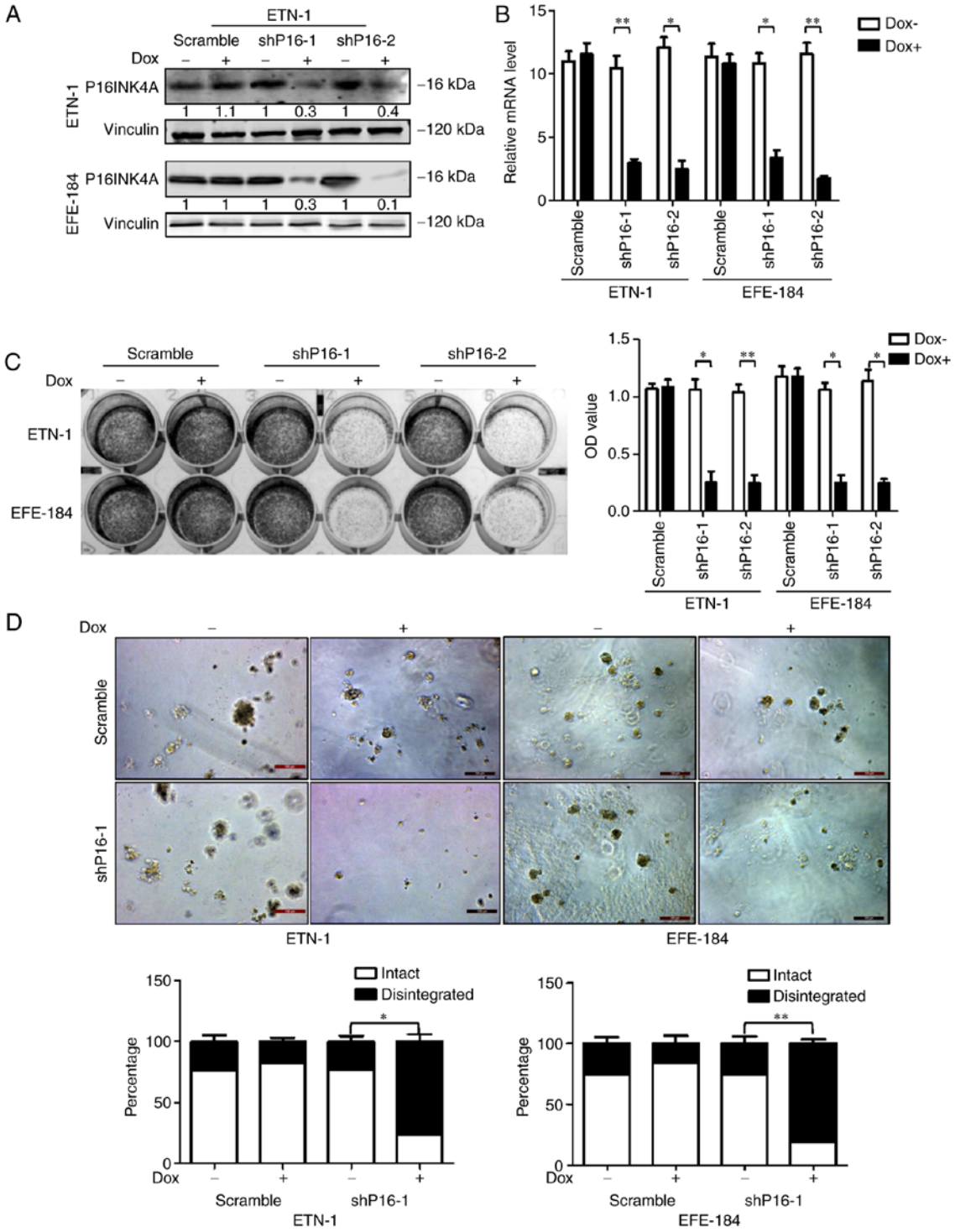

Figure 2. Effects of P16INK4A knockdown on the proliferation of ETN-1 and EFE-184. (A) Western blot analysis and (B) relative mRNA level of P16INK4A in doxycycline inducible scramble ETN-1, shP16-1 ETN-1 and shP16-2 ETN-1, and scramble EFE-184, shP16-1 EFE-184 and shP16-2 EFE-184 cells. Vinculin was used as a loading control. (C) Colony-forming assay of inducible scramble or shP16 ETN-1 and EFE-184 cells treated with or without doxycycline. The cells were seeded in 24-well plates with or without doxycycline and cultured for 10 days. Cells were stained with crystal violet solution at the time of harvest. Means ± standard deviation for 3 independent experiments are depicted. *P<0.05 and **P<0.01 (Student's t-test). (D) Inducible scramble or shP16 ETN-1 and EFE-184 cells with or without doxycycline were maintained in 3D culture medium for 96 h. Representative images of scored structures (intact or disintegrated) are depicted in this panel. Scale bar, 50 μm. *P<0.05 and **P<0.01 (Student's t-test). P16INK4A, cyclin-dependent kinase inhibitor 2A; shP16, short hairpin P16INK4A; Dox, doxycycline; OD, optical density.

potential of ETN-1 and EFE-184 cells was significantly decreased, as depicted in 2D colony-forming and 3D culture assays (Fig. 2C and D). A wound healing assay also demonstrated that cells with P16INK4A knocked down exhibit significantly reduced migration ability, compared with those with intact P16INK4A expression (Fig. 3). These results indicated that P16INK4A, in addition to its canonical role as a tumor suppressor, may also serve an oncogenic role in P16INK4A-positive cells, although the underlying mechanism remains elusive.

Table I. Different expression of P16INK4A between tumor samples of USCs and UECs.

Investigator	Year	P16INK4A positive in USCs (%)	P16INK4A positive in UECs (%)	Method	P-value	Refs no.
Yemelyanova *et al*	2009	95 (47/49)	38 (38/101)	IHC	<0.01	(8)
Netzer *et al*	2011	78 (24/31)	35 (11/31)	IHC	<0.001	(24)
Levine DA *et al*	2013	31 (31/101)	2.9 (13/447)	mRNA, RPPA	<0.01	(26)
Han *et al*	2013	80 (12/15)	11 (5/43)	IHC	<0.001	(25)
Chen *et al*	2017	92 (48/52)	26 (17/65)	IHC	<0.01	(9)
Xiao *et al*	2017	75 (25/33)	12 (11/88)	IHC	<0.01	Present study

IHC, immunohistochemistry; P16INK4A, cyclin-dependent kinase inhibitor 2A; UEC, uterine endometroid carcinoma; USC, uterine serous carcinoma; RPPA, the reverse phase protein array.

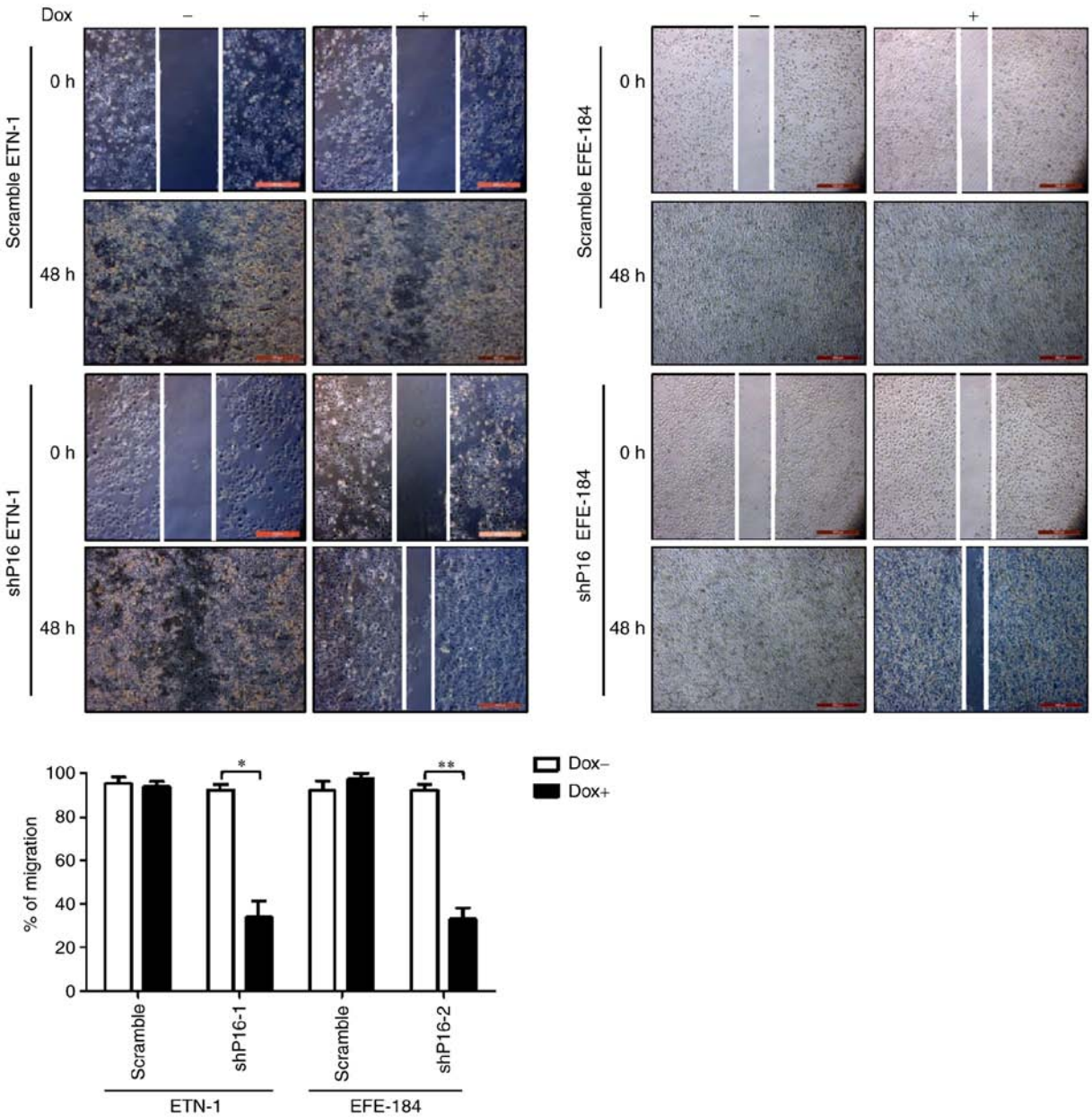

Figure 3. Effects of P16INK4A knockdown on the migration of ETN-1 and EFE-184. Cell migration was determined with a wound healing assay. Images of the wound areas were captured at 0 and 48 h (magnification, x200; scale bar, 100 μm). Means ± standard deviation for 3 independent experiments are depicted. *P<0.05 and **P<0.01 (Student's t-test). P16INK4A, cyclin-dependent kinase inhibitor 2A; shP16, short hairpin P16INK4A; Dox, doxycycline.

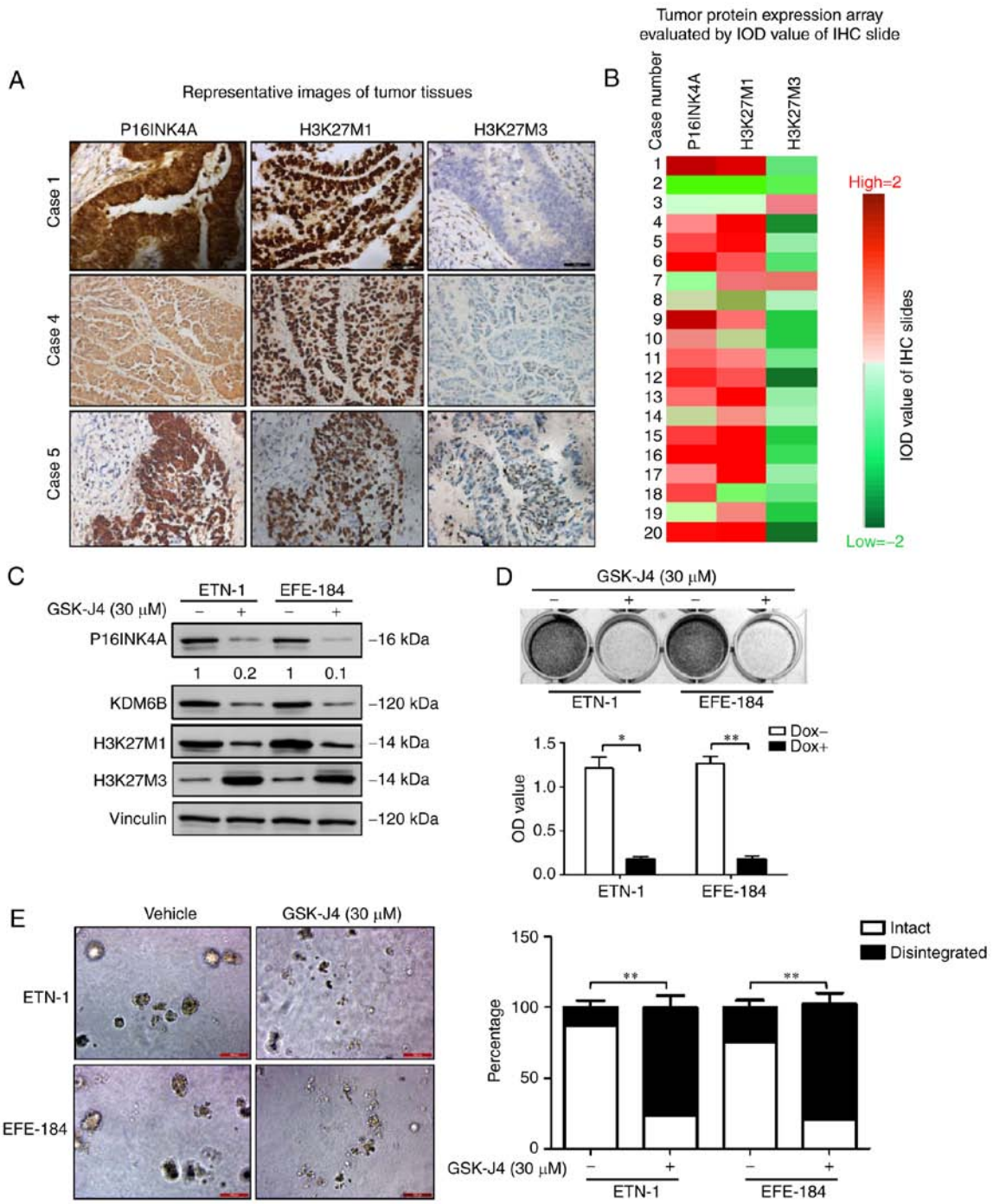

Figure 4. P16INK4A overexpression coexists with demethylation of H3K27 in endometrial cancer, and the effects of target inhibition of H3K27 demethylation on cellular P16INK4A and growth potential of ETN-1 and EFE-184 cells. (A) Representative images for IHC analyses in 3 independent cases. H3K27M1, H3K27M3 and P16INK4A were evaluated in these tumor samples. Scale bar, 50 μm. (B) A total of 70% (14/20) of uterine serous carcinoma samples in the study cohort were H3K27M3-negative and H3K27M1-positive. Hotmap was depicted according to the IOD value of each slides [ranging from -2 (green) to +2 (red)], red indicates positive staining and green represents negative staining. (C) Western blot analyses of P16INK4A, H3K27M1 and H3K27M3 in ETN-1 and EFE-184 cells when left untreated or treated with vehicle (DMSO) and GSK-J4 (30 μM). Vinculin was used as a loading control. (D) ETN-1 cells were treated with DMSO and GSK-J4 (30 μM) for 5 days. Means ± standard deviation for 3 independent experiments are depicted. *P<0.05; **P<0.01 (Student's t-test). (E) The ETN-1 and EFE-184 cells treated with DMSO and GSK-J4 (30 μM) were maintained in 3D culture medium for 4 days. Representative images of scored structures (intact vs. disintegrated) are depicted. Scale bar, 100 μm. **P<0.01 (Student's t-test). DMSO, dimethyl sulfoxide; P16INK4A, cyclin-dependent kinase inhibitor 2A; H3K27, histone 3 lysine 27; KDM6B, histone lysine demethylase 6B; IHC, immunohistochemistry; IoD, integrated option density; OD, optical density.

P16INK4A overexpression in USCs coexists with the demethylation of H3K27. Previous studies demonstrated that the transcription of *P16INK4A* is primarily regulated by the methylation level of H3K27 in cervical cancer (14,28,29). To determine whether a similar mechanism is involved in the abundant expression of P16INK4A in USC, 20 cases of P16INK4A-positive USC tissue samples was investigated. Using IHC, 70% (14/20) samples in this cohort were identified as H3K27M3-negative and H3K27M1-positive (Fig. 4A and B). A similar result was also observed in the ETN-1 and EFE-184

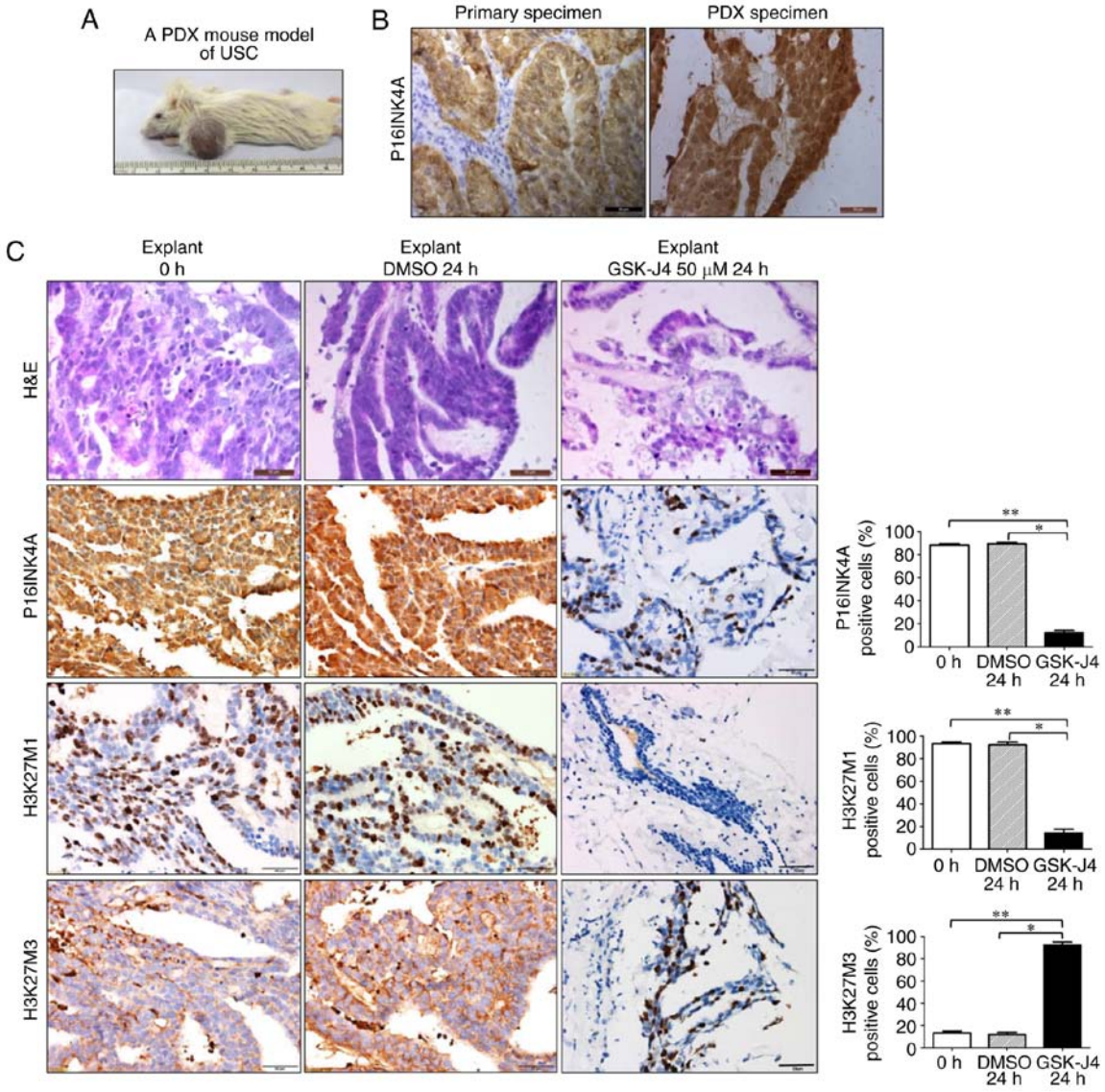

Figure 5. Target inhibition of H3K27 demethylation by GSK-J4 exerts therapeutic effects on USC PDX tumor explants. (A) Establishment of a PDX mouse model with a USC tumor. (B) Representative P16INK4A staining images of human primary specimen and tumor from the PDX mouse model. Scale bar, 50 μm. (C) Representative H&E and immunohistochemistry staining images of P16INK4A, H3K27M1 and H3K27M3 on tumor explants when left untreated or treated with DMSO or GSK-J4 (50 μM). The expression of P16INK4A and H3K27M1 was significantly reduced, while H3K27M3 staining was significantly increased in GSK-J4-treated explants, compared with the tissues treated by vehicle or untreated. Scale bar, 50 μm. *P<0.05 and **P<0.01 [analysis of variance and a post hoc test (Student-Newman-Keuls)]. H&E, hematoxylin and eosin; P16INK4A, cyclin-dependent kinase inhibitor 2A; H3K27, histone 3 lysine 27; DMSO, dimethyl sulfoxide; PDX, patient-derived xenograft; USC, uterine serous carcinoma.

cell lines. Western blot analysis revealed weak H3K27M3 and robust H3K27M1 expression in ETN-1 and EFE-184 cancer cells (Fig. 4C). These observations indicate that the upregulation of P16INK4A in USC may share the same mechanism as reported in cervical cancer aforementioned.

KDM6B inhibition reduces P16INK4A expression and suppresses the proliferation of cancer cells in cell lines and USC explants. As histone KDM6B mediates H3K27 demethylation and increases the expression of P16INK4A (11,14), it was hypothesized that treatment with the KDM6B inhibitor GSK-J4 may be effectively used to target P16INK4A-positive cancer cells. As expected, GSK-J4 treatment significantly suppressed cell growth, compared with the control vehicle (Fig. 4D), which was also verified in 3D culture assays (Fig. 4E). Furthermore, following GSK-J4 treatment, P16INK4A expression was markedly inhibited with the increase of H3K27M3 and the decrease of KDM6B and H3K27M1 (Fig. 4C), supporting our hypothesis that target inhibition of H3K27 demethylation is a potential treatment for P16INK4A-positive endometrial cancer.

To further confirm the treatment effects *ex vivo*, a PDX mouse model of USC was then established (Fig. 5A). The model maintained a number of histopathological characteristics of the human primary tumor, including P16INK4A overexpression (Fig. 5B). In the *ex vivo* experiment, following GSK-J4 treatment, samples were subjected to histological examination. It was observed that, following treatment with GSK-J4, cellular integrity was markedly disrupted, without distinct USC-specific structures. However, explants treated with DMSO retained the architecture and cellularity of non-treated tumors. IHC analysis also demonstrated that the

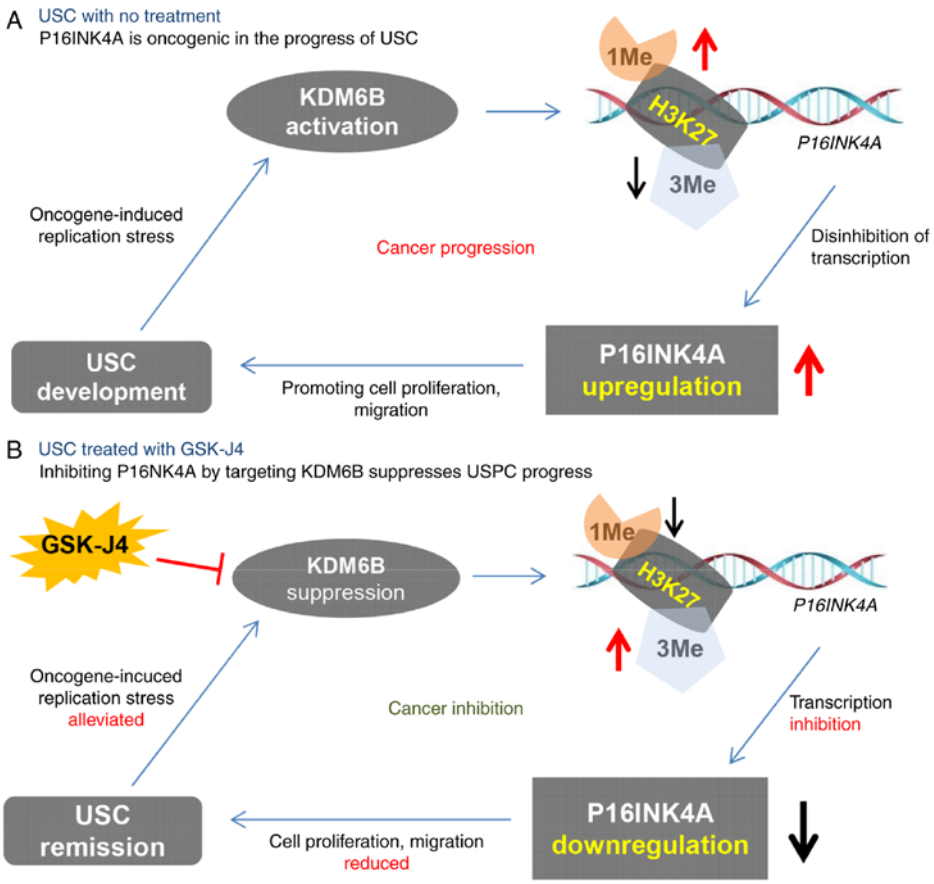

Figure 6. Graphical summary of the present study. (A) When USC is left untreated, P16INK4A serves an oncogenic role promoting endometrial cancer progression. (B) When USC is treated with GSK-J4, cancer progression is suppressed by P16INK4A through targeting KDM6B. USC, uterine serous cancer; *P16INK4A*, cyclin-dependent kinase inhibitor 2A; H3K27, histone 3 lysine 27; KDM6B, histone lysine demethylase 6B.

expression of P16INK4A and H3K27M1 was significantly reduced, while H3K27M3 staining was significantly increased in GSK-J4-treated explants (Fig. 5C). The results from the tumor explants were consistent with those obtained from cell lines, indicating that targeting KDM6B by GSK-J4 may be a viable treatment strategy for P16INK4A-positive endometrial cancer cases.

Discussion

To the best of our knowledge, the present study is the first to investigate the oncogenic role of P16INK4A in endometrial cancer. The present data demonstrated that P16INK4A is able to promote proliferation of endometrial cancer cells, and targeting P16INK4A by altering H3K27 methylation may be a beneficial strategy for the treatment of endometrial cancer.

Contrary to the known role of P16INK4A as a tumor suppressor, the present study revealed its oncogenic effects. In a previous review, the mechanism underlying P16INK4A overexpression in cancer includes P16INK4A-CDK4/6-Rb pathway alterations, such as the E7 of human papillomavirus (HPV) targeting RB (13); however, in endometrial cancer, this may not be the case. Firstly, there is no evidence that endometrial cancer is associated with HPV infection, and secondly, there are few mutations or mRNA changes in downstream molecules, such as CDK4/6 and RB, in endometrial cancer, as detailed in The Cancer Genome Atlas database (26).

As aforementioned, a number of previous independent reports support the present conclusions. The studies on cervical and hepatic cancer demonstrate that P16INK4A is necessary for cell survival and migration (10,11). These studies further indicated that the oncogenic role of P16INK4A is dependent on its inhibition of CDK4/6 (10,11). Additionally, researchers also identified that different cellular P16INK4A localization may be associated with different biological functions. It has been demonstrated that cytoplasmic P16INK4A expression is frequently associated with poor survival in head and neck (30), and breast cancer (31), and cytoplasmic P16INK4A can promote cell proliferation and migration via a cell cycle-unrelated pathway (32). In the present study, P16INK4A was overexpressed in the nucleus and cytoplasm of USC cells, and following GSK-J4-induced P16INK4A depletion, cancer cell proliferation and migration were markedly reduced. Thus, the oncogenic role P16INK4A in endometrial cancer may be mediated through its classic CDK4/6 inhibitory effect on the nucleus and an uncertain cell cycle-unrelated pathway in the cytoplasm.

Another observation of the present study was how P16INK4A is overexpressed in endometrial cancer. Consistently with a previous report (14), this upregulation of P16INK4A also results from demethylation of H3K27. Based on this observation, it appeared reasonable to develop a strategy for USC treatment by inhibiting P16INK4A through targeting KDM6B. The present experiments, consistent with

previous studies (14,33-35), revealed strong treatment effects of GSK-J4 on ETN-1 cells and USC explants. Thus, the present study not only revealed the role of demethylation of H3K27 in the progression of endometrial cancer, but also indicated a novel targeting strategy for the treatment of USC. The content of the present study is graphically summarized in Fig. 6.

There were certain limitations to the present study. Firstly, as relatively few endometrial cell lines were P16INK4A-positive, only ETN-1 and EFE-184 cells were included in the experiments aforementioned. Further research should be performed on more P16INK4A-positive cell lines in order to verify these conclusions. Another weakness is that the effects of GSK-J4 was only tested on cell lines and *ex vivo* tissues. Animal studies should be performed in the future to further confirm the validity of this treatment strategy. The third controversial issue is about the concentration of GSK-J4 (30 μM), which was a slightly increased, compared with other common small molecular inhibitors. However, this concentration had been frequently used in a number of studies on cervical cancer (11), brain glioma (34) and immunologic diseases (36,37), demonstrating that this concentration of GSK-J4 exerted prominent *in vitro* and *in vivo* anti-proliferative effects on cancerous and non-cancerous cells and tissues.

In conclusion, despite certain limitations, the present results revealed an oncogenic role of the traditional tumor suppressor P16INK4A in endometrial cancer, indicating a possible novel approach to developing promising therapeutic paradigms for P16INK4A-positive USC.

Acknowledgements

The authors would like to thank Dr Yuan Zhang, Dr Jinglei Ding and Dr Penglong Cao (Dalian Medical Univercity, Dalian, China), for their help and support in our experiments and manuscript preparation.

Funding

The present study was supported by the National Natural Science Foundation of China (grant nos. 81372853 and 81572586 to P.L.), Liaoning Provincial Climbing Scholars Supporting Program of China (grant no. 2012086524 to P.L.), Provincial Natural Science Foundation of Liaoning (grant no. 2014023002 to P.L.) and Youth Natural Science Foundation of First Affiliated Hospital of Dalian Medical University (grant no. 2014QN003/2017FH004 to Z.X.).

Availability of data and materials

The datasets used and/or analyzed during the present study are available from the corresponding author on reasonable request.

Authors' contributions

ZX, YH, HS and PL are responsible for the conception and design of the study. ZX, YH, CL, PL, LX, JY and MW performed the majority of the cell experiments. ZX, YH, PL and HS performed the acquisition of data, and provided animals, facilities and selected the patients. ZX, YH, CL, TS, HS and PL performed the writing, review and revision of the manuscript. ZX, YH, CL, LX, JY, MW, YX, TS, PL and LS performed the animal-model establishments and *ex vivo* experiments. YH, CL, ZX, LS and YX performed the H&E and IHC staining, and examinations. All authors read and approved the final manuscript.

Ethics approval and consent to participate

The study and the use of human samples were approved by the ethics committee of First Affiliated Hospital of Dalian Medical University (Dalian, China). The use of experimental animals was approved by the ethics committee of Dalian Medical University and strictly followed the guideline for tumor induction in mice and rats. Written informed consent was obtained from the patient.

Patient consent for publication

The authors declared that the patients provided written informed consent for the publication of the associated data in this manuscript.

Competing interests

The authors declare that they have no competing interests.

References

1. Siegel RL, Miller KD and Jemal A: Cancer statistics, 2016. CA Cancer J Clin 66: 7-30, 2016.
2. Wright JD, Barrena Medel NI, Sehouli J, Fujiwara K and Herzog TJ: Contemporary management of endometrial cancer. Lancet 379: 1352-1360, 2012.
3. Salvesen HB, Haldorsen IS and Trovik J: Markers for individualised therapy in endometrial carcinoma. Lancet Oncol 13: e353-e361, 2012.
4. Asghar U, Witkiewicz AK, Turner NC and Knudsen ES: The history and future of targeting cyclin-dependent kinases in cancer therapy. Nat Rev Drug Discov 14: 130-146, 2015.
5. Sherr CJ, Beach D and Shapiro GI: Targeting CDK4 and CDK6: From discovery to therapy. Cancer Discov 6: 353-367, 2016.
6. Witkiewicz AK, Knudsen KE, Dicker AP and Knudsen ES: The meaning of $p16^{ink4a}$ expression in tumors: Functional significance, clinical associations and future developments. Cell Cycle 10: 2497-2503, 2011.
7. Halperin R, Zehavi S, Habler L, Hadas E, Bukovsky I and Schneider D: Comparative immunohistochemical study of endometrioid and serous papillary carcinoma of endometrium. Eur J Gynaecol Oncol 22: 122-126, 2001.
8. Yemelyanova A, Ji H, Shih IeM, Wang TL, Wu LS and Ronnett BM: Utility of p16 expression for distinction of uterine serous carcinomas from endometrial endometrioid and endocervical adenocarcinomas: Immunohistochemical analysis of 201 cases. Am J Surg Pathol 33: 1504-1514, 2009.
9. Chen W, Husain A, Nelson GS, Rambau PF, Liu S, Lee CH, Lee S, Duggan MA and Köbel M: Immunohistochemical profiling of endometrial serous carcinoma. Int J Gynecol Pathol 36: 128-139, 2017.
10. Chen YW, Chu HC, Ze-Shiang Lin, Shiah WJ, Chou CP, Klimstra DS and Lewis BC: p16 Stimulates CDC42-dependent migration of hepatocellular carcinoma cells. PLoS One 8: e69389, 2013.
11. McLaughlin-Drubin ME, Park D and Munger K: Tumor suppressor $p16^{INK4A}$ is necessary for survival of cervical carcinoma cell lines. Proc Natl Acad Sci USA 110: 16175-16180, 2013.
12. Pauck A, Lener B, Hoell M, Kaiser A, Kaufmann AM, Zwerschke W and Jansen-Dürr P: Depletion of the cdk inhibitor $p16^{INK4a}$ differentially affects proliferation of established cervical carcinoma cells. J Virol 88: 5256-5262, 2014.

13. Romagosa C, Simonetti S, Lopez-Vicente L, Mazo A, Lleonart ME, Castellvi J and Ramon y Cajal S: $p16^{Ink4a}$ overexpression in cancer: A tumor suppressor gene associated with senescence and high-grade tumors. Oncogene 30: 2087-2097, 2011.
14. McLaughlin-Drubin ME, Crum CP and Munger K: Human papillomavirus E7 oncoprotein induces KDM6A and KDM6B histone demethylase expression and causes epigenetic reprogramming. Proc Natl Acad Sci USA 108: 2130-2135, 2011.
15. Junttila TT, Akita RW, Parsons K, Fields C, Lewis Phillips GD, Friedman LS, Sampath D and Sliwkowski MX: Ligand-independent HER2/HER3/PI3K complex is disrupted by trastuzumab and is effectively inhibited by the PI3K inhibitor GDC-0941. Cancer Cell 15: 429-440, 2009.
16. Liu P, Cheng H, Santiago S, Raeder M, Zhang F, Isabella A, Yang J, Semaan DJ, Chen C, Fox EA, *et al*: Oncogenic PIK3CA-driven mammary tumors frequently recur via PI3K pathway-dependent and PI3K pathway-independent mechanisms. Nat Med 17: 1116-1120, 2011.
17. Juvekar A, Burga LN, Hu H, Lunsford EP, Ibrahim YH, Balmana J, Rajendran A, Papa A, Spencer K, Lyssiotis CA, *et al*: Combining a PI3K inhibitor with a PARP inhibitor provides an effective therapy for BRCA1-related breast cancer. Cancer Discov 2: 1048-1063, 2012.
18. Livak KJ and Schmittgen TD: Analysis of relative gene expression data using real-time quantitative PCR and the $2^{-\Delta\Delta CT}$ method. Methods 25: 402-408, 2001.
19. Lee GY, Kenny PA, Lee EH and Bissell MJ: Three-dimensional culture models of normal and malignant breast epithelial cells. Nat Methods 4: 359-365, 2007.
20. Li L, Chang W, Yang G, Ren C, Park S, Karantanos T, Karanika S, Wang J, Yin J, Shah PK, *et al*: Targeting poly(ADP-ribose) polymerase and the c-Myb-regulated DNA damage response pathway in castration-resistant prostate cancer. Sci Signal 7: ra47, 2014.
21. Xiao Y, Wang J, Qin Y, Xuan Y, Jia Y, Hu W, Yu W, Dai M, Li Z, Yi C, *et al*: Ku80 cooperates with CBP to promote COX-2 expression and tumor growth. Oncotarget 6: 8046-8061, 2015.
22. Morton CL and Houghton PJ: Establishment of human tumor xenografts in immunodeficient mice. Nat Protoc 2: 247-250, 2007.
23. Wang D, Li C, Zhang Y, Wang M, Jiang N, Xiang L, Li T, Roberts TM, Zhao JJ, Cheng H, *et al*: Combined inhibition of PI3K and PARP is effective in the treatment of ovarian cancer cells with wild-type *PIK3CA* genes. Gynecol Oncol 142: 548-556, 2016.
24. Netzer IM, Kerner H, Litwin L, Lowenstein L and Amit A: Diagnostic implications of p16 expression in serous papillary endometrial cancer. Int J Gynecol Cancer 21: 1441-1445, 2011.
25. Han G, Sidhu D, Duggan MA, Arseneau J, Cesari M, Clement PB, Ewanowich CA, Kalloger SE and Köbel M: Reproducibility of histological cell type in high-grade endometrial carcinoma. Modern Pathol 26: 1594-1604, 2013.
26. Cancer Genome Atlas Research Network, Kandoth C, Schultz N, Cherniack AD, Akbani R, Liu Y, Shen H, Robertson AG, Pashtan I, Shen R, Benz CC, *et al*: Integrated genomic characterization of endometrial carcinoma. Nature 497: 67-73, 2013.
27. Konecny GE, Winterhoff B, Kolarova T, Qi J, Manivong K, Dering J, Yang G, Chalukya M, Wang HJ, Anderson L, *et al*: Expression of p16 and retinoblastoma determines response to CDK4/6 inhibition in ovarian cancer. Clin Cancer Res 17: 1591-1602, 2011.
28. Groves IJ, Knight EL, Ang QY, Scarpini CG and Coleman N: HPV16 oncogene expression levels during early cervical carcinogenesis are determined by the balance of epigenetic chromatin modifications at the integrated virus genome. Oncogene 35: 4773-4786, 2016.
29. Soto DR, Barton C, Munger K and McLaughlin-Drubin ME: KDM6A addiction of cervical carcinoma cell lines is triggered by E7 and mediated by $p21^{CIP1}$ suppression of replication stress. PLoS Pathog 13: e1006661, 2017.
30. Zhao N, Ang MK, Yin XY, Patel MR, Fritchie K, Thorne L, Muldrew KL, Hayward MC, Sun W, Wilkerson MD, *et al*: Different cellular $p16^{INK4a}$ localisation may signal different survival outcomes in head and neck cancer. Br J Cancer 107: 482-490, 2012.
31. Di Vinci A, Perdelli L, Banelli B, Salvi S, Casciano I, Gelvi I, Allemanni G, Margallo E, Gatteschi B and Romani M: $p16^{INK4a}$ promoter methylation and protein expression in breast fibroadenoma and carcinoma. Int J Cancer 114: 414-421, 2005.
32. Gray-Schopfer VC, Cheong SC, Chong H, Chow J, Moss T, Abdel-Malek ZA, Marais R, Wynford-Thomas D and Bennett DC: Cellular senescence in naevi and immortalisation in melanoma: A role for p16? Br J Cancer 95: 496-505, 2006.
33. Hashizume R, Andor N, Ihara Y, Lerner R, Gan H, Chen X, Fang D, Huang X, Tom MW, Ngo V, *et al*: Pharmacologic inhibition of histone demethylation as a therapy for pediatric brainstem glioma. Nat Med 20: 1394-1396, 2014.
34. Cregan S, Breslin M, Roche G, Wennstedt S, MacDonagh L, Albadri C, Gao Y, O'Byrne KJ, Cuffe S, Finn SP, *et al*: Kdm6a and Kdm6b: Altered expression in malignant pleural mesothelioma. Int J Oncol 50: 1044-1052, 2017.
35. Morozov VM, Li Y, Clowers MM and Ishov AM: Inhibitor of H3K27 demethylase JMJD3/UTX GSK-J4 is a potential therapeutic option for castration resistant prostate cancer. Oncotarget 8: 62131-62142, 2017.
36. Kruidenier L, Chung CW, Cheng Z, Liddle J, Che K, Joberty G, Bantscheff M, Bountra C, Bridges A, Diallo H, *et al*: A selective jumonji H3K27 demethylase inhibitor modulates the proinflammatory macrophage response. Nature 488: 404-408, 2012.
37. Wu W, Qin M, Jia W, Huang Z, Li Z, Yang D, Huang M, Xiao C, Long F, Mao J, *et al*: Cystathionine-γ-lyase ameliorates the histone demethylase JMJD3-mediated autoimmune response in rheumatoid arthritis. Cell Mol Immunol: May 29, 2018 (Epub ahead of print). doi: 10.1038/s41423-018-0037-8.